ACS APPLIED MATERIALS & INTERFACES

Research Article

www.acsami.org

A Detailed Investigation on the Interactions between Magnetic Nanoparticles and Cell Membrane Models

Thiers Massami Uehara,[†,‡] Valeria Spolon Marangoni,[†] Nicholas Pasquale,[‡] Paulo Barbeitas Miranda,[†] Ki-Bum Lee,[‡] and Valtencir Zucolotto*[,†]

[†]Nanomedicine and Nanotoxicology Group, Physics Institute of São Carlos, University of São Paulo, CP 369, São Carlos, São Paulo, Brazil 13566-590

[‡]Department of Chemistry and Chemical Biology, Rutgers University, 610 Taylor Road, Piscataway, New Jersey 08854-8058, United States

Supporting Information

ABSTRACT: The understanding of the interactions between small molecules and magnetic nanoparticles is of great importance for many areas of bioapplications. Although a large array of studies in this area have been performed, aspects involving the interaction of magnetic nanoparticles with phospholipids monolayers, which can better mimic biological membranes, have not yet been clarified. This study was aimed at investigating the interactions between Langmuir films of dipalmitoyl phosphatidylglycerol and dipalmitoyl phosphatidylcholine, obtained on an aqueous subphase, and magnetic nanoparticles. Sum-frequency generation (SFG) vibrational spectroscopy was used to verify the orientation and molecular conformation and to better understand the interactions between phospholipids and the magnetic nanoparticles. Surface pressure−area isotherms and SFG spectroscopy made it possible to investigate the interaction of these nanomaterials with components of phospholipids membranes at the water surface.

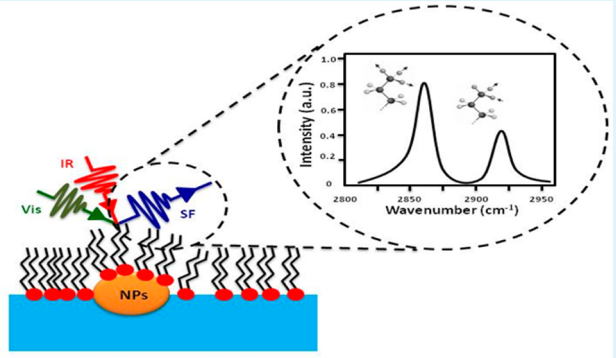

KEYWORDS: *nanomedicine, nanotoxicology, magnetic nanoparticles, Langmuir films, SFG spectroscopy*

1. INTRODUCTION

In recent years, magnetic nanoparticles (MNP) have generated great interest in the nanosciences because of their unique physicochemical properties, and have been applied to many areas, such as information storage,[1] color imaging,[2] microwave absorption,[3] sensors,[4] and nanomedicine.[5−9] In the field of nanomedicine, in particular, iron oxide nanoparticles (Fe_2O_3 and Fe_3O_4) have shown increasing potential as promising tools demonstrating a myriad of biological applications such as magnetic resonance imaging (MRI), drug delivery[5] and therapies based on hyperthermia.[6] Several efforts have been made in fabricating stable colloidal iron oxide solutions with superior physical properties, including biocompatibility and good dispersivity, which are critical for biomedical applications. Currently, several groups reported that the properties of MNPs depend on particle size, dispersivity, crystallinity, chemical composition, and surface coating.[10,11]

Enormous advances have been made using various formulations and further functionalizations of iron oxide nanoparticles to improve their dispersivity and biocompatibility with specific surface coatings, including ligand exchange to generate hydrophilic particles, ligand conjugation, and micelle encapsulation.[12−14] Iron oxide nanoparticles functionalized with dextran,[15] liposomes,[8] dendrimers,[9] and poly(ethylene glycol) have been widely applied as imaging contrast agents, which show high efficacy in enhancing images and enabling the detection of local lesions in living subjects through noninvasive, real-time magnetic resonance imaging (MRI).[16]

Currently, intensive research is underway to understand the interactions between magnetic nanoparticles and biological systems, which is necessary to optimize their diagnostic sensitivity and therapeutic capabilities, as well as their biocompatibility and mechanism of action, which involves the interactions between nanomaterials and small molecules.[17,18] Different in vitro studies have shown that surface chemistry, particles size, and morphology greatly affects the interactions between nanoparticles and plasma proteins, interact with plasma proteins, which subsequently affects cellular uptake, toxicity and molecular responses.[19−26] Because cellular uptake of nanomaterials involves, in the first stages, any type of interaction between the nanomaterial and the cellular membrane, knowledge about these interactions is crucial to

Received: September 17, 2013
Accepted: December 3, 2013
Published: December 3, 2013

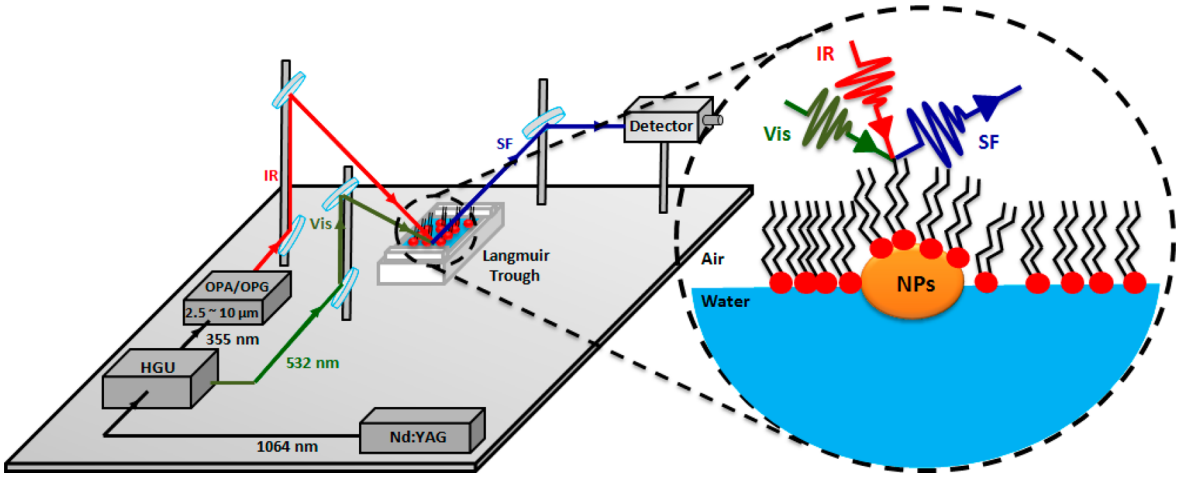

Figure 1. Layout of an SFG spectroscopy coupled to a Langmuir trough, representing the overlap of the beams (IR and visible) to generate the sum-frequency signal.

the understanding of the mechanisms related to cell uptake. Perspectives on the practical applications of this study include the design of specific materials capable of interacting—or not—with cell membranes, for applications in nanomedicine[27] and toxicological investigations.[28]

Recently, our group developed a new strategy to evaluate the interaction and toxicity of nanoparticles using Langmuir films.[29] This technique yields high-quality organized ultrathin films composed of different types of lipids, proteins, and sterols, which can serve as models of cellular membranes.[30,31] However, the study of the interactions between magnetic nanoparticles with model cell membranes has not been reported.

In this study, Langmuir films of dipalmitoyl phosphatidylglycerol (DPPG) and dipalmitoylphosphatidyl choline (DPPC) were fabricated and allowed to interact with iron oxide (Fe_3O_4) nanoparticles stabilized with poly(diallydimethylammonium chloride) (PDAC), (Fe_3O_4–PDAC) and dextran (Fe_3O_4-dextran). The presence of stabilizers mediated the interactions of the nanoparticles with the lipidic membranes. The membrane systems were characterized using the sum-frequency generation vibrational spectroscopy (SFG spectroscopy),[32,33] a nonlinear optical technique used to study surfaces and interfaces in situ. The understanding of the interactions between magnetic nanoparticles and mimetic cell membranes is relevant for several technological and research areas, including nanoparticle-assisted drug delivery[34] and cancer therapy.[35]

2. SFG SPECTROSCOPY

SFG is a technique with surface specificity and chemical selectivity capable of obtaining vibrational spectra of species at surfaces and interfaces.[36−42] SFG is a second-order nonlinear optical process in which two input laser beams, one in the visible (Vis) and another on the infrared (IR), overlap spatially and temporally at a surface to generate a coherent beam signal at the sum frequency of the input beams. The source of the sum-frequency photons is the second-order polarization induced by IR and VIS electric fields, $E_j(\omega_{vis})$ and $E_k(\omega_{IR})$, respectively:

$$P_i^{(2)}(\omega_{SF}) = \chi_{ijk}^{(2)}(\omega_{SF} = \omega_{Vis} + \omega_{IR}) : E_j(\omega_{Vis})E_k(\omega_{IR}) \quad (1)$$

where $\chi_{ijk}^{(2)}$ is the second-order susceptibility tensor of the medium (the indices *ijk* are the Cartesian coordinates *x*, *y*, *z*). Because $\chi_{ijk}^{(2)}$ is zero in a centrosymmetric medium (within the electric-dipole approximation), SFG occurs only at a surface or interface where the inversion symmetry is broken.[42] The latter makes the technique highly surface-specific, allowing one to obtain information of a thin interfacial layer without interference from the bulk response. The vibrational spectrum of the interface is obtained by tuning the IR frequency through resonances of the surface molecules, which leads to an enhancement of $\chi^{(2)}$, and therefore of the SFG signal intensity.

3. EXPERIMENTAL SECTION

$FeSO_4 \cdot 7H_2O$ from Baker, $FeCl_3$ anhydrous from VETEC, PDAC (M_w: 400 000−500 000) and dextran (M_w: 40 000) from Aldrich were used without additional purification. DPPG and DPPC (≥ 99%) were acquired from Avanti Polar Lipids.

PDAC-stabilized Fe_3O_4 nanoparticles were synthesized according to a method previously described.[44] The Fe_3O_4-dextran nanoparticles were prepared using exactly the same methodology and concentrations, upon replacing the cationic polymer PDAC for the anionic dextran.

DPPG and DPPC Langmuir films were obtained in a minitrough housed in a class 10 000 clean room. The aqueous subphase was supplied by a Mili-Q purification system from Milipore, containing sodium phosphate monobasic solution and sodium phosphate dibasic solution (Sigma-Aldrich >99% purity), both with a concentration of 1×10^{-1} mol/L. All measurements were carried out at 22 °C.

For Langmuir films formation, a typical concentration of DPPG and DPPC was 0.5 mg/mL, diluted in chloroform. The volume spread on the surface of the aqueous subphase was 16 μL, followed by a 10 min incubation time in which the solvent was evaporated and the molecules spread at the surface. The formation of DPPG and DPPC domains on the films at the water surface was verified using Brewster Angle Microscopy (BAM), model BAM2 PLUS − Nanofilm Technology, Germany.

The Langmuir minitrough was coupled to the SFG spectrometer for in situ measurements. The same procedure used in the clean room was repeated to characterize the monolayer via SFG. The SFG spectra were taken with a commercial SFG spectrometer (EKSPLA, Lithuania). Briefly, an active-passive model locked Nd^{+3}: YAG laser generates 30 ps pulses at a wavelength of 1064 nm, with a repetition rate of 20 Hz. It pumps a Harmonic Generator Unit (HGU) that produces the second- and third-harmonic (532 nm and 355 nm, respectively). Part of the visible beam (532 nm) is used to excite the sample, together with a tunable IR pulse (from 4000 to 1000 cm^{-1}, 3

cm^{-1} resolution) generated by an Optical Parametric Generator/Optical Parametric Amplifier (OPG/OPA) pumped at 355 nm, coupled to a Difference Frequency Generation stage (DFG) which is pumped by 1064 nm. The visible and IR pulses overlap spatially and temporally at the interface, generating the SFG signal in the reflection geometry. The incidence angles of the IR, visible and SFG beam were, respectively, 55, 61, and ~60°. The overlap spot area of the pump beams (visible and infrared) on the sample was approximately 1 mm^2, and the pulse energies were 750 and 160 μJ for the visible and infrared beams, respectively. The polarization combination used in all measurements was the SSP, referring to the beams: SFG, visible and infrared, respectively. Polarization S and P represents the component of electric field which are perpendicular and parallel to the incidence plane, respectively.[41] A Langmuir trough, with an area of 5 × 19.5 cm^2, was coupled to the SFG spectrometer to enable in situ measurements (Figure 1). All SFG spectra were collected at a surface pressure of 40 mN m^{-1}. Before the surface pressure reaches the maximum value ($\Pi \sim$ 40 mN/m, before the collapse of the monolayer) the barrier movement was stopped to initiate the acquisition of the SFG spectrum. The spectra were acquired in a frequency range from 2500–3100 cm^{-1} with 3 cm^{-1} steps.

The SFG spectra were collected after the incorporation of Fe_3O_4-dextran, Fe_3O_4-PDAC, dextran, or PDAC in the subphase of the DPPG or DPPC films. An incubation time of 10 min was used in all measurements.

4. RESULTS AND DISCUSSION

The morphology of the DPPG and DPPC Langmuir films at the water surface is shown in Figure 2. The BAM images allow for the verification of ultrathin films formation in the water subphase with low surface pressure (7 and 10.8 mN/m, respectively).

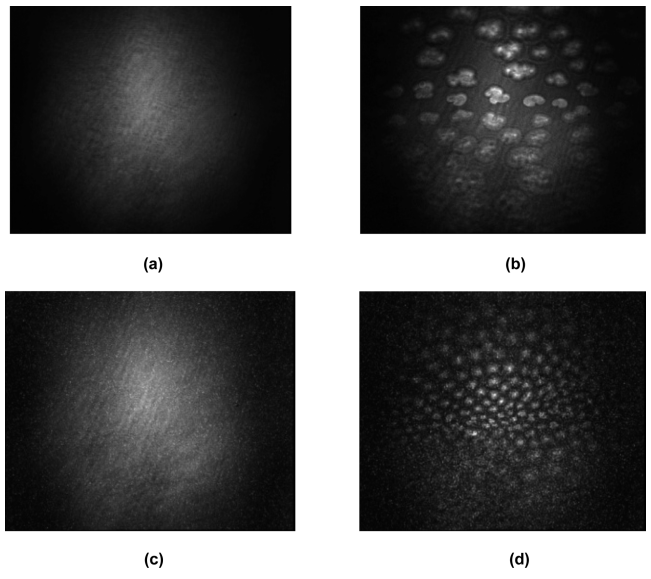

Figure 2. BAM images from films formed at the air–water interface. DPPG: (a) π = 0 mN/m and (b) π = 7 mN/m. DPPC: (c) π = 0 mN/m and (d) 10.8 mN/m.

Panels a and b in Figure 3 represent, respectively, the isotherms from DPPG and DPPC monolayers containing Fe_3O_4-dextran, Fe_3O_4-PDAC, dextran, and PDAC in the subphase. In Figure 3a, we verify that the isotherms from monolayers incubated with DPPG and Fe_3O_4-PDAC shifted to higher values of area per molecule, compared to the neat DPPG isotherm. This effect was not observed for monolayers in contact with dextran or Fe_3O_4-dextran nanoparticles, indicating that the interaction between of these materials and the membrane is not strong enough to cause a reorganization of the phospholipid molecules in the membrane.

A different behavior was found for the DPPC system, as shown in Figure 3b. The isotherms for monolayers in contact with both types of nanoparticles and with pure PDAC displaced to smaller areas per molecule. In contrast, the system in contact with pure dextran did not present a significant shift.

The isotherm for each system is affected by the type and magnitude of interactions between phospholipids and magnetic nanoparticles. SFG spectroscopy was used as an additional tool to elucidate the possible ways the nanoparticles interact with the phospholipids monolayers, leading to the changes observed in the isotherms of Figure 3. The rationale behind this idea is to characterize the possible arrangements and conformation of alkyl chains of DPPG and DPPC at the air–water interface, and to correlate them to the variations observed in the isotherms of Figure 3. Panels a and b in Figure 4 represent the spectra of DPPG and DPPC on an aqueous subphase.

The spectra in panels a and b in Figure 4 are dominated by resonances at 2879 and 2945 cm^{-1}, which are assigned to the symmetric stretch of CH_3 from alkyl chains of phospholipids and its Fermi resonance with the symmetric CH_3 bending mode, respectively.[43] Because no CH_2 stretches from alkyl chains appear in the spectra, they must adopt a centrosymmetric arrangement and it is possible to conclude that the phospholipid film is highly organized with the alkyl chains in the all-trans conformation, forming a compact monolayer over the aqueous subphase.[43]

SFG spectra of DPPG monolayers in the presence of iron oxide nanoparticles are shown in Figure 5. The absence of the CH_2 symmetric stretch at 2850 cm^{-1} in all spectra indicates that the monolayers remain organized at the air-water interface, with well-packed all-trans alkyl chains. This organization appears even for the systems containing PDAC, which expand the isotherms, as shown in Figure 3. It is important to note that at the high pressures at which the SFG spectra were acquired (~40 mN/m) there is not much difference in the area per molecule for DPPG on different subphases, except with the presence of Fe_3O_4-PDAC. Therefore, the observed changes in intensity among the spectra of Figure 5 probably reflect the uncertainty in the measurement and are not significant. Consequently, the SFG spectra provide evidence that the membrane remains organized even after incorporation of the Fe_3O_4-PDAC and pure PDAC.

The proposed arrangement for the interaction of the pure PDAC and Fe_3O_4–PDAC is illustrated in Figure 6. In this case, the compounds incorporate into the membrane and occupy a larger area per molecule (as shown in isotherms) and the alkyl chains of the phospholipids remain well-packed and oriented at the air-water interface, in a way that only CH_3 stretching modes are detected in the SFG spectra, according to the data of Figure 5. Pure PDAC also presents the same behavior, but the shift is smaller due to the difference in size compared to the NPs, as observed in Figure 3a. However, for the dextran compounds, no difference was observed in the isotherms (Figure 3a) or in the SFG spectra (Figure 5) in the presence of DPPG (negatively charged). This is expected due the negative charge of dextran at neutral pH. Consequently, dextran and Fe_3O_4-dextran did not interact with the DPPG and remain in the aqueous subphase. Consequently, the interaction between the NPs, or the free polymer and the DPPG monolayer is driven by an electrostatic mechanism.

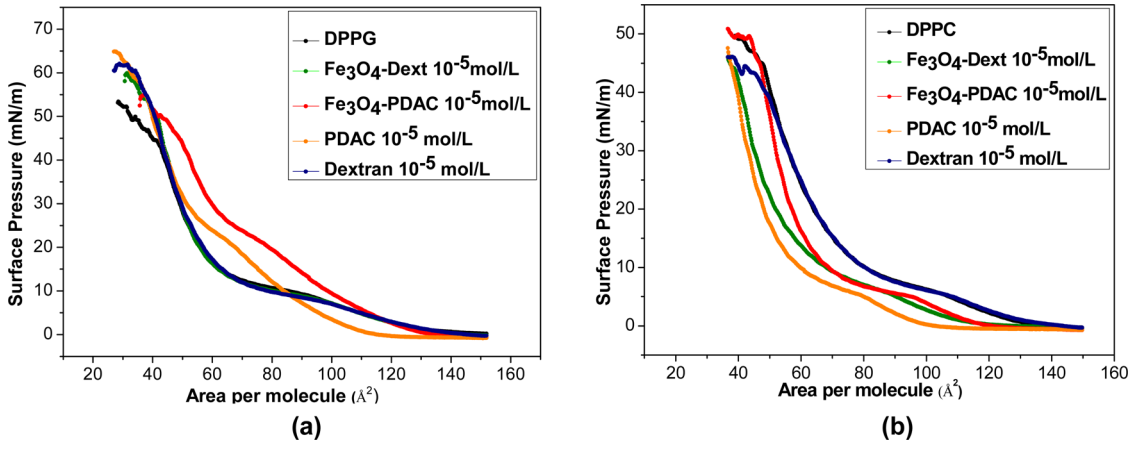

Figure 3. Isotherms for (a) DPPG and (b) DPPC systems in the presence of nanoparticles and stabilizers.

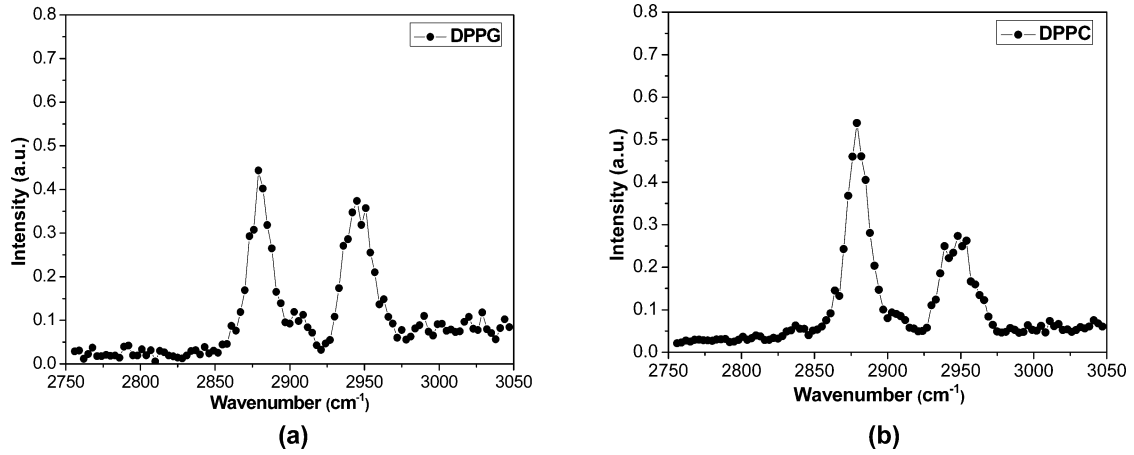

Figure 4. SFG spectra on neat monolayers: (a) DPPG and (b) DPPC .

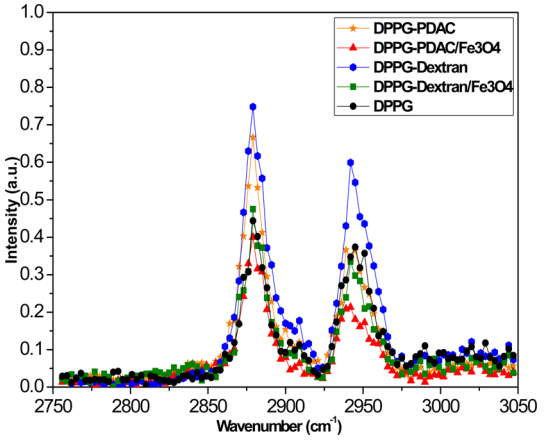

Figure 5. SFG spectra for DPPG monolayers after incubation with nanoparticles and stabilizers.

The spectra of DPPC and iron oxide nanoparticles are shown in Figure 7. In these spectra, again only the CH_3 stretching modes of the alkyl chains are detected, and the alkyl chains of phospholipids also remain distended at the air−water interface, as in the case of DPPG.

In the case of DPPC monolayers, according to the isotherms depicted in Figure 3b, there is a decrease in the area per molecule after incorporation of nanoparticles and/or pure PDAC. A possible scenario in this case would be the PDAC-NPs interacting and removing DPPC molecules from the air-water interface, as shown in Figure 8. The interaction occurs via immobilization of DPPC around the nanoparticles, which dislocates them to the hydrophobic side of the monolayer, as in collapsed lipid domains. This arrangement also explains the trends for the SFG intensities in Figure 7. For the three systems where monolayer condensation was observed in Figure 3b − with PDAC and with both NPs − an increase in SFG signal should be expected because of the increases in monolayer

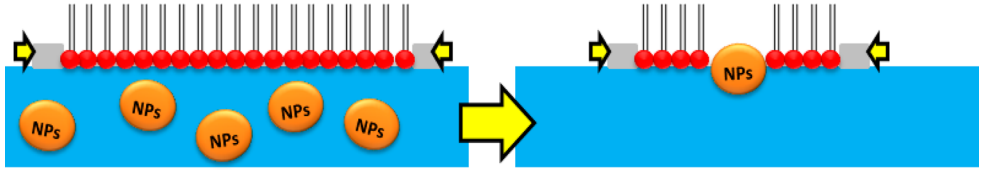

Figure 6. Schematic illustration of the sequence of interactions between the DPPG monolayers and the nanoparticles at the air−water interface.

dx.doi.org/10.1021/am404042r | ACS Appl. Mater. Interfaces 2013, 5, 13063−13068

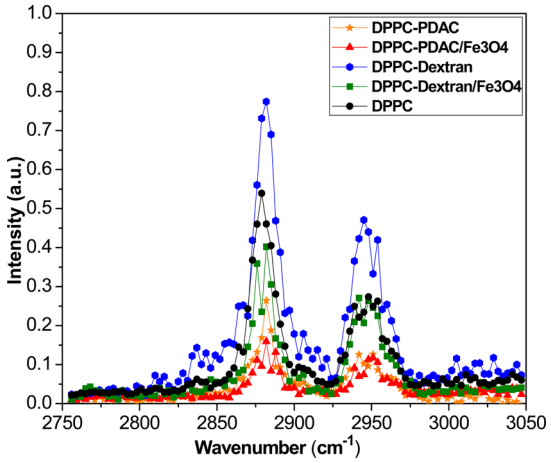

Figure 7. SFG spectra for DPPC monolayers after incubation with nanoparticles and stabilizers.

density. However, a decrease in intensity is observed for these systems in comparison with DPPC-dextran or pure DPPC. This may be due to a partial cancellation of the CH_3 signal of the compact DPPC monolayer (which should be the same for all cases) by that of CH_3 groups around the NPs on the overlayer, with a net contribution facing down the DPPC monolayer.

The effect in the DPPC isotherms (Figure 3b) was the same for dextran- and PDAC-stabilized NPs. This is expected because DPPC is zwitterionic. However, for pure polymers, the effect was different, suggesting that not only the electrostatic effect is important but also the size of the compounds.

5. CONCLUSION

Langmuir films represent an efficient cell membrane mimetic model, in which it is possible to incorporate nanomaterials to investigate the detailed interactions capable of occurring between the monolayer and the nanomaterials. According to our findings, functionalized superparamagnetic nanoparticles are able to spontaneously interact with DPPG and DPPC monolayers. In the former, positively charged nanoparticles incorporate in the negatively charged membrane, remaining at the interface, which leads to an increase in the values of area per molecule. In the NPs/DPPC system, the nanoparticles are capable of interacting with the zwitterionic DPPC molecules, forming an overlayer of lipid-covered NPs on top of the DPPC film, which leads to a reduction of the area per molecule, as observed in the isotherms. These findings open new possibilities for investigating the interactions involving cell membrane models with different NPs and molecules. The results can be interesting for future investigations in fields such as drug delivery, nanomedicine, and nanotoxicology.

■ ASSOCIATED CONTENT

Supporting Information

Additional information on size distribution and zeta potential for all nanoparticles used in the interactions study. This material is available free of charge via the Internet at http://pubs.acs.org/.

■ AUTHOR INFORMATION

Corresponding Author

*E-mail: zuco@ifsc.usp.br.

Notes

The authors declare no competing financial interest.

■ ACKNOWLEDGMENTS

The authors thank FAPESP, Capes, and FINEP for the financial support.

■ REFERENCES

(1) Chakraborty, A. *J. Magn. Magn. Mater.* **1999**, *32*, 57−60.
(2) Ziolo, R. F. Developer composition containing superparamagnetic polymers. U.S. 4474866-A, 02 Oct 1984 198442.
(3) Liu, J.; Che, R.; Chen, H.; Zhang, F.; Xia, F.; Wu, Q.; Wang, M. *Small* **2012**, *8*, 1214−1221.
(4) Sljukic, B.; Banks, C. E.; Compton, R. G. *Nano Lett.* **2006**, *6*, 1556−1558.
(5) Piao, Y.; Kim, J.; Bin Na, H.; Kim, D.; Baek, J. S.; Ko, M. K.; Lee, J. H.; Shokouhimehr, J.; Hyeon, M.; Wrap-Bake-Peel, T. *Nat. Mater.* **2008**, *7*, 242−247.
(6) Sonvico, F.; Mornet, S.; Vasseur, S.; Dubernet, C.; Jaillard, D.; Degrouard, J.; Hoebeke, J.; Duguet, E.; Colombo, P.; Couvreur, P. *Bioconjugate Chem.* **2005**, *16*, 1181−1188.
(7) Xie, J.; Wang, J. H.; Niu, G.; Huang, J.; Chen, K.; Li, X. G.; Chen, X. Y. *Chem. Commun.* **2010**, *46*, 433−435.
(8) Bruns, O. T.; Ittrich, H.; Peldschus, K.; Kaul, M. G.; Tromsdorf, U. I.; Lauterwasser, J.; Nikolic, M. S.; Mollwitz, B.; Merkell, M.; Bigall, N. C. *Nat. Nanotechnol.* **2009**, *4*, 193−201.
(9) Shi, X. Y.; Wang, S. H.; Swanson, S. D.; Ge, S.; Cao, Z. Y.; Van Antwerp, M. E.; Landmark, K. J.; Baker, J. R. *Adv. Mater.* **2008**, *20*, 1671−1678.
(10) Duan, H. W.; Kuang, M.; Wang, X. X.; Wang, Y. A.; Mao, H.; Nie, S. M. *J. Phys. Chem. C* **2008**, *112*, 8127−8131.
(11) Tromsdorf, U. I.; Bigall, N. C.; Kaul, M. G.; Bruns, O. T.; Nikolic, M. S.; Mollwitz, B.; Sperling, R. A.; Reimer, R.; Hohenberg, H.; Parak, W. J. *Nano Lett.* **2007**, *7*, 2422−2427.
(12) Gupta, A. K.; Gupta, M. *Biomaterials* **2005**, *26*, 3995−4021.
(13) Latham, A. H.; Williams, M. E. *Acc. Chem. Res.* **2008**, *41*, 411−420.

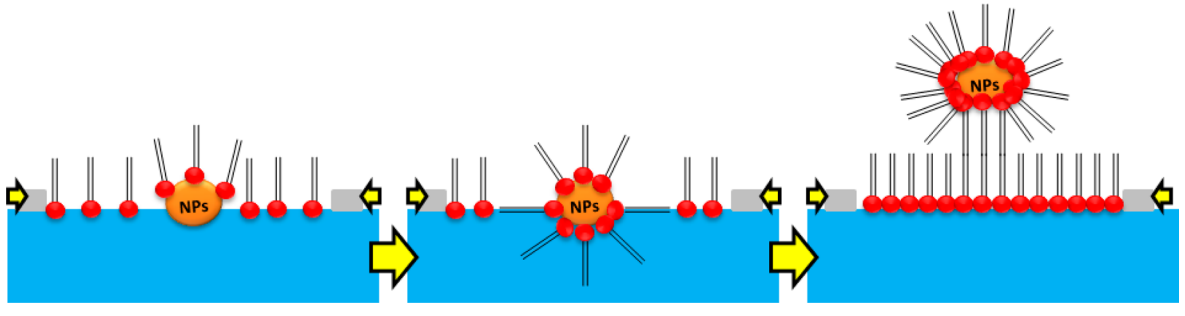

Figure 8. Schematic illustration of the sequence of interactions between the DPPC monolayers and the nanoparticles at the air−water interface.

(14) Amstad, E.; Zurcher, S.; Mashaghi, A.; Wong, J. Y.; Textor, M.; Reimhult, E. *Small* **2009**, *5*, 1334−1342.
(15) Wong, R. M.; Gilbert, D. A.; Liu, K.; Louie, A. Y. *ACS Nano* **2012**, *6*, 3461−3467.
(16) Huang, J.; Bu, L.; Xie, J.; Chen, K.; Cheng, Z.; Li, X.; Chen, X. *ACS Nano* **2010**, *4*, 7151−7160.
(17) Katagiri, K.; Nakamura, M.; Koumoto, K. *ACS Appl. Mater. Interfaces* **2010**, *2*, 768−773.
(18) Li, L.; Köpf, M. H.; Gurevich, S. V.; Friedrich, R.; Chi, L. *Small* **2012**, *8*, 488−503.
(19) Luciani, N.; Gazeau, F.; Wilhelm, C. J. *Mater. Chem.* **2009**, *19*, 6373−6380.
(20) Thorek, D. L. J.; Tsourkas, A. *Biomaterials* **2008**, *29*, 3583−3590.
(21) Verma, A.; Stellacci, F. *Small* **2010**, *6*, 12−21.
(22) Jiang, W.; Kim, B. Y. S.; Rutka, J. Y.; Chan, W. C. W. *Nat. Nanotechnol.* **2008**, *3*, 145−150.
(23) He, C. B.; Hu, Y. P.; Yin, L. C.; Tang, C.; Yin, C. H. *Biomaterials* **2010**, *31*, 3657−3666.
(24) Osaki, F.; Kanamori, T.; Sando, S.; Sera, T.; Aoyama, Y. J. *Am. Chem. Soc.* **2004**, *126*, 6520−6521.
(25) Chithrani, B. D.; Ghazani, A. A.; Chan, W. C. W. *Nano Lett.* **2006**, *6*, 662−668.
(26) Yan, L.; Zhao, F.; Li, S.; Hu, Z.; Zhao, Y. *Nanoscale* **2011**, *3*, 362−382.
(27) Cancino, J.; Nobre, T. M.; Oliveira, O. N., Jr.; Machado, S. A. S.; Zucolotto, V. *Nanotoxicology* **2013**, *7*, 61−70.
(28) Roberts, G. *Langmuir-Blodgett Films*; Plenum Press: New York, 1990.
(29) Petty, M. C. *Langmuir-Blodgett Films: An Introduction*; Cambridge University Press: Cambridge, U.K., 1996.
(30) Boyd, R. W. *Nonlinear Optics*; Academic Press: Burlington, MA, 2004.
(31) Shen, Y. R. *Proc. Natl. Acad. Sci. U.S. A.* **1996**, *93*, 12104−12111.
(32) Wang, Y. E.; Zhang, H.; Fan, Q.; Neal, C. R.; Zuo, Y. Y. *Soft Matter* **2012**, *8*, 504−511.
(33) Preetha, A.; Huilgol, N.; Banerjee, R. *Biomed. Pharmacothe.* **2005**, *59*, 491−497.
(34) Lai, P.; Nathoo, S.; Ku, T.; Gill, S.; Azarmi, S.; Roa, W.; Lobenberg, R.; Prenner, E. J. *J. Biomed. Nanotechnol.* **2010**, *6*, 145−152.
(35) Lystvet, S. M.; Volden, S.; Halskau, O.; Glomm, W. R. *Soft Matter* **2011**, *7*, 11501−11509.
(36) Miranda, P. B.; Du, Q.; Shen, Y. R. *Chem. Phys. Lett.* **1998**, *286*, 1−8.
(37) Shen, Y. R. *Surf. Sci.* **1994**, *299-300*, 551−562.
(38) Bain, C. D. *J. Chem. Soc.-Faraday Trans.* **1995**, *91*, 1281−1296.
(39) Eisenthal, K. B. *Chem. Rev.* **1996**, *96*, 1343−1360.
(40) Du, Q.; Superfine, R.; Freysz, E.; Shen, Y. R. *Phys. Rev. Lett.* **1997**, *119*, 6144−6152.
(41) Shen, Y. R. *Annu. Rev. Phys. Chem.* **1989**, *40*, 327−350.
(42) Lambert, A. G.; Davies, P. B.; Neivandt, D. J. *Appl. Spectrosc. Rev.* **2005**, *40*, 103−145.
(43) Guyot-Sionnest, P.; Hunt, J. H.; Shen, Y. R. *Phys. Rev. Lett.* **1987**, *59*, 1597−1600.
(44) Marangoni, V. S.; Martins, M. V. A.; Souza, J. A.; Oliveira, O. N.; Zucolotto, V.; Crespilho, F. N. *J. Nanopart. Res.* 2012, *14*.